Supramolecular Chemistry

International Edition: DOI: 10.1002/anie.201903045
German Edition: DOI: 10.1002/ange.201903045

Rotaxane Probes for the Detection of Hydrogen Peroxide by ^{129}Xe HyperCEST NMR Spectroscopy

*Sarah H. Klass, Ashley E. Truxal, Tahoe A. Fiala, Joseph Kelly, Dang Nguyen, Joel A. Finbloom, David E. Wemmer, Alexander Pines, and Matthew B. Francis**

Abstract: *The development of sensitive and chemically selective MRI contrast agents is imperative for the early detection and diagnosis of many diseases. Conventional responsive contrast agents used in ^{1}H MRI are impaired by the high abundance of protons in the body. ^{129}Xe hyperCEST NMR/MRI comprises a highly sensitive complement to traditional ^{1}H MRI because of its ability to report specific chemical environments. To date, the scope of responsive ^{129}Xe NMR contrast agents lacks breadth in the specific detection of small molecules, which are often important markers of disease. Herein, we report the synthesis and characterization of a rotaxane-based ^{129}Xe hyperCEST NMR contrast agent that can be turned on in response to H_2O_2, which is upregulated in several disease states. Added H_2O_2 was detected by ^{129}Xe hyperCEST NMR spectroscopy in the low micromolar range, as well as H_2O_2 produced by HEK 293T cells activated with tumor necrosis factor.*

The sensitive and selective detection of disease markers is of high importance for the identification and treatment of a variety of human diseases. Magnetic resonance imaging (MRI), the clinical version of nuclear magnetic resonance (NMR) spectroscopy, is a non-invasive imaging technique that can achieve high resolution and excellent tissue penetration. Conventional MRI techniques rely on differences in the relaxation properties of protons primarily associated with water molecules in different tissue types. Typically, contrast agents in the form of paramagnetic metal chelates or spin-labeled biomolecules alter the relaxation properties of local water molecules to provide additional structural and functional information.[1] Responsive ^{1}H and ^{13}C NMR contrast agents have also been developed that produce a signal only in the presence of particular disease markers, such as enzymes, signaling molecules, and oxidizing conditions.[2–5] This approach can aid in early disease detection and provides insight into the chemical environment, ultimately enabling a better understanding of disease pathology. However, even with these contrast agents, signal and sensitivity are often lost due to spectral complexity within the limited chemical shift range that protons possess.

Hyperpolarized xenon chemical exchange saturation transfer (^{129}Xe hyperCEST) NMR spectroscopy comprises a sensitive complement to traditional ^{1}H MR imaging approaches.[6] Although it is a nontoxic and nonreactive noble gas, xenon is very sensitive to its local chemical environment due to its high electron polarizability. The easy deformation of its electron cloud leads to chemical shifts that range over several hundred ppm in biological samples, thereby enabling direct and quantitative imaging of local spin environments that are often indistinguishable by conventional MRI.[7] The combination of this acute sensitivity and xenon's high solubility in blood, tissue, and lipophilic membranes distinguishes it from other heteronuclear contrast agents.[8] Furthermore, facile hyperpolarization of ^{129}Xe nuclei can be obtained through spin-exchange optical pumping, thereby leading to contrast enhancements of 4–5 orders of magnitude over thermal polarization.[9] The lack of background ^{129}Xe signals in most systems gives rise to uncomplicated spectra as well as the potential for improved resolution of small, localized populations of target molecules.[10]

Being chemically inert, ^{129}Xe is effectively functionalized for selective detection by participating in supramolecular host–guest interactions, which can cause either large chemical shifts or changes in relaxation parameters that are distinct to the host environments in which ^{129}Xe resides.[7,11–13] Since the majority of xenon atoms are present in bulk solution and undergo continuous exchange with host molecules, we can exploit the exchange between host-bound and "free" xenon by way of CEST techniques to attain detection limits of hosts down to sub-nanometer levels.[14,15]

To create "turn-on" ^{129}Xe hyperCEST NMR contrast agents, researchers have used the known Xe host cucurbit-[6]uril (CB6) because of its favorable exchange parameters for hyperCEST applications.[15,16] CB6 is a toroidal molecule that can harbor a single ^{129}Xe atom in its interior cavity, which creates a distinct ^{129}Xe@CB6 chemical shift.[17] CB6 has been used as an in vivo contrast agent in rat vasculature, highlighting the applicability of future designs based on this moiety.[18] To prevent ^{129}Xe molecules from entering the interior of CB6 and producing this unique signal until desired, the CB6 can be threaded onto a molecular axle. This axle is then capped by two bulky stopper groups to create a supramolecular species known as a rotaxane.[19,20] By designing one of these bulky stoppers to be cleaved under specific conditions, such as activation by a disease marker, a Xe@CB6

[*] S. H. Klass, A. E. Truxal, T. A. Fiala, J. Kelly, D. Nguyen, J. A. Finbloom, D. E. Wemmer, A. Pines, Prof. M. B. Francis
Department of Chemistry
University of California, Berkeley (USA)
A. Pines, Prof. M. B. Francis
Materials Sciences Division
Lawrence Berkeley National Laboratories
Berkeley, California 94720 (USA)
E-mail: mbfrancis@berkeley.edu

Supporting information (including full experimental methods) can be found in the Supporting Information and the ORCID identification numbers for some of the authors of this article can be found under: https://doi.org/10.1002/anie.201903045.

signal can be selectively observed only when activated. Using these design principles, our group and others have previously produced rotaxanes and rotaxane-like species where the CB6 response is occluded by a molecular species threaded through the cavity. These systems have been designed to release CB6 under a variety of conditions, such as strong base,[14] cancer-related matrix-metalloproteinase (MMP) enzymes,[21] and the human carbonic anhydrase enzyme.[22] This "turn on" effect differs in concept from other systems, such as the previously reported biotinylated CB7 construct, which exhibits a unique NMR shift upon binding to its protein target.[23] In other studies, cyclodextrin-based pseudorotaxanes have also provided encouraging results.[24]

Based on the design elements of these first examples, we sought to create a probe that would be responsive to increased levels of hydrogen peroxide (H_2O_2, Figure 1). Prior research has implicated upregulated levels of H_2O_2 production in the advancement of inflammation, and increases in oxidative stress have been correlated with the advancement of cancer,[25] diabetes,[26] cardiovascular disease, pulmonary disease, muscle atrophy,[29] and wound healing.[30,31] The high sensitivity of ^{129}Xe hyperCEST NMR spectroscopy could allow the detection of extracellular H_2O_2 at the low physiological levels (0.5–50 μM) associated with these disease states.[32,30]

^{129}Xe MRI has demonstrated a unique strength in functional lung imaging, making oxidatively sensitive sensors most

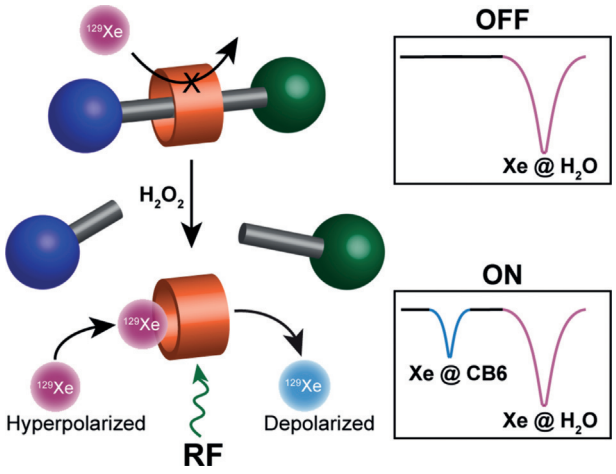

Figure 1. Hydrogen peroxide sensing rotaxane for ^{129}Xe hyperCEST NMR spectroscopy. CB6 (orange) is threaded along a molecular axle (gray) that is mechanically locked into place by the presence of two bulky stoppers (blue and green), thereby creating a supramolecular complex known as a rotaxane. The presence of the axle in the interior of CB6 prevents Xe from entering the cavity and thus no Xe@CB6 signal is observed in the hyperCEST NMR spectrum (OFF). After cleavage of one of the bulky stoppers by a reaction with H_2O_2, the CB6 cavity becomes available to form a host–guest complex with Xe atoms. Insets: When inside the CB6 cavity, the Xe experiences a relatively shielded environment, creating a unique chemical shift observable by Xe NMR spectroscopy. A radiofrequency (RF) saturation pulse corresponding to this chemical shift can be applied to depolarize the Xe selectively inside the CB6. The reduction of the bulk hyperpolarized Xe (Xe@H_2O) signal as a result of depolarizing xenon at the Xe@CB6 chemical shift is then observed (ON). Recording the Xe@H_2O signals using an array of saturation frequencies yields the above *z*-spectra.

provocative for the detection of pulmonary afflictions in which abnormally increased levels of H_2O_2 have been linked. Known examples include chronic obstructive pulmonary disease, community-acquired pneumonia, cancer of the lung, and denervation-induced muscle atrophy.[18–20] Current examples for imaging H_2O_2 in vivo or in opaque environments include chemiluminescent nanoparticles, a ^{13}C-labeled MRI probe, and a bioluminescent reporter.[4,33,34] However, these techniques suffer from either limited sensitivity or the requirement of modifying the natural sample environment. Therefore, imaging H_2O_2 in an unperturbed environment at physiologically relevant concentrations remains an interesting challenge. Herein we describe the first synthesis, characterization, and application of a ^{129}Xe hyperCEST contrast agent for the detection of H_2O_2.

Several design elements were considered in the synthesis of a rotaxane that could function as a ^{129}Xe hyperCEST turn-on probe in response to H_2O_2: 1) Inspired by the design of several H_2O_2-activated fluorescent, positron emission tomography (PET), and ^{1}H/^{13}C MRI probes, we incorporated a sensitive and selective aryl boronic acid group as a cleavable cap on the rotaxane (Figure 2a);[32,34–37] 2) to improve the sensitivity, the rotaxane axle was composed of a *p*-xylenediamine moiety, which has one of the lowest reported K_a values for CB6 ($5.5\times10^2\,M^{-1}$, Figure 2b);[19] 3) to allow for ease of synthesis and modification to the rotaxane design, a convergent route was designed, in which the axle and cap were joined at later steps (Figure 2c). Using this route, two such rotaxanes were prepared with differing nonresponsive capping moieties. Rotaxane **1** was capped with a fluorophore to allow specific UV detection during HPLC/LC-MS cleavage studies (Figure 2d). Rotaxane **2** was capped with a maleimide functional group that allows further conjugation to biomolecules and was used in the ^{129}Xe hyperCEST experiments (Figure 2e). Both molecules were purified using reverse-phase HPLC (RP-HPLC) before use.

To determine the cleavage rates of the rotaxane caps in the presence of excess H_2O_2, a sample of rotaxane **1** was monitored over time by HPLC/LC-MS. Rotaxane **1** was found to be completely oxidized within 1 h. However, the 1,6-elimination reaction that ultimately results in bond cleavage proved to be the slow step, with less than 50% cleavage after 16 h. Kinetic measurements extrapolated from these data (assuming pseudo-first-order conditions with 7.5 μM rotaxane **1** and 100 μM H_2O_2 in 1xPBS (PBS = phosphate buffered saline) buffer at pH 7.4) gave a rate constant of $k = 8.52\times10^{-3}\,s^{-1}$ (Figure 3).

To determine if the sucessful cleavage reaction observed using LC-MS resulted in a ^{129}Xe hyperCEST signal, multiple concentrations of rotaxane **2** and H_2O_2 were analyzed to monitor the emergence of the Xe@CB6 signal over time. A Xe@CB6 hyperCEST response evolved within 1 h following the addition of 2 equivalents of hydrogen peroxide (25 μM rotaxane **2**, 50 μM H_2O_2), and quickly reached and maintained an apparent maximum saturation of about 25% (Figure 4a). Previous rotaxane-based sensors have required 8–24 h to demonstrate the same magnitude of CEST response, thus demonstrating the notable improvement in efficiency and sensitivity of this system.[14,21] Evaluation of rotaxane **2**

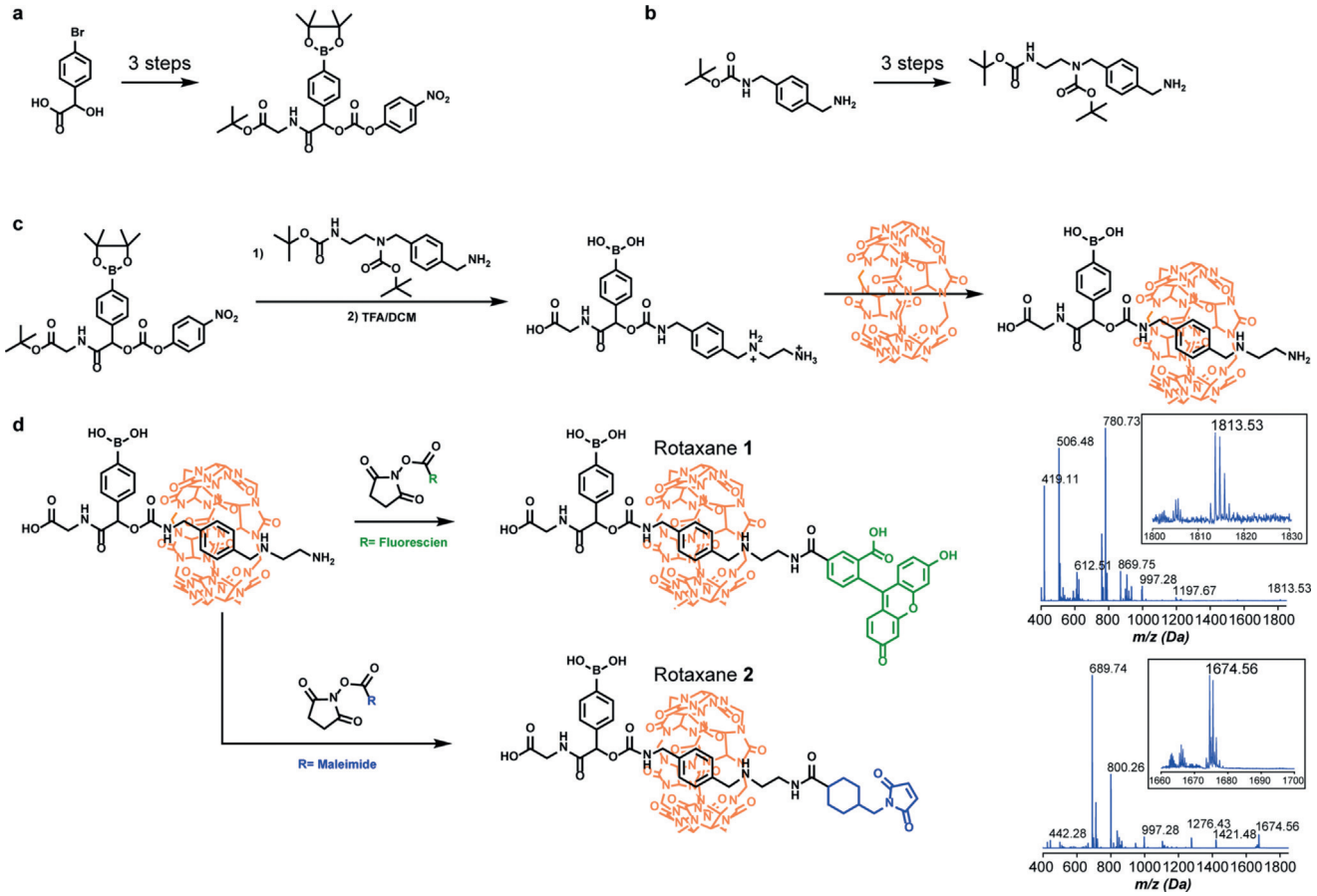

Figure 2. Convergent synthesis of rotaxanes **1** and **2**. a) The synthetic route to produce a H_2O_2-sensing cap involved three steps, and b) the synthetic route to produce a *para*-xylenediamine axle required four steps. c) The two segments were combined using a two-step procedure and subsequently threaded with CB6. d) The axles were then capped with either fluorophore or maleimide functionalities to give rotaxanes **1** and **2** respectively. LC-MS traces are shown for rotaxane **1** (expected *m*/*z*: 1813.44; observed *m*/*z*: 1813.53, boron isotope pattern observed) and rotaxane **2** (expected *m*/*z*: 1674.37; observed *m*/*z*: 1674.56, boron isotope pattern observed).

(Figure 4b) and H_2O_2 at various concentrations (Figure 4c) led to detection limits of 2.5 μM and 5 μM, respectively. Notably, the limits of detection could be significantly improved by new advancements in hyperpolarization methods, where ^{129}Xe hyperpolarization levels of greater than 50% have been obtained.[38] This is a large enhancement over the polarization levels used in this study, which were only 0.05–2%.

Although the observed response magnitudes did increase with increasing rotaxane **2** or H_2O_2 concentration, they did not seem to be able to achieve more than 25–28% saturation. In contrast, a 5 μM solution of free CB6 that was not previously threaded onto a rotaxane provided nearly complete saturation immediately using the same acquisition parameters. One explanation for the incomplete saturation could be the formation of a complex between the carbonyl-rich portal of CB6 and the protonated amine remaining at the end of the cleaved rotaxane. CB6 is known to form such complexes with short peptides as well as long diammonium alkanes.[39–41] This includes the *p*-xylylenediamine group used in this study.[19] Indeed, we can observe an intact Pseudorotaxane **4** complex by HPLC/LCMS after cleavage of the axle by H_2O_2. Furthermore, the mass spectra indicate that H_2O_2 does not affect the molecular structure of the CB6 or the cleaved axle. Presumably the interaction with the cleaved axle sequesters some of the CB6, thus limiting the saturation level that is observed. Nonetheless, the successful acquisition of a Xe@CB6 response indicates that enough CB6 is released for xenon exchange into and out of the cavity.

The maleimide cap on rotaxane **2** enabled the functionalization of cysteine residues present on the vascular cell adhesion molecule (VCAM)-1 binding peptide and a tobacco mosaic virus (TMV) protein based nanoparticle. The VCAM-1 binding peptide was chosen because this receptor has implications in inflammatory disease and cancer.[42,43] TMV is a disk-shaped nanoparticle that assembles into a nanoscale structure that is 17 nm in diameter and composed of 34 protein monomers.[44] This protein assembly was chosen for is distinct morphology, which could be adventageous in drug delivery and imaging applications.[45,46] When using excess rotaxane **2**, the VCAM-1 peptide was completly modified, while the TMV nanoparticle was purposefully modified at 30% of its available sites, thereby resulting in 10 rotaxane molecules per TMV disk (Figure S1).

We then sought to detect endogenously produced H_2O_2 by exposing HEK 293T cells to tumor necrosis factor alpha (TNF), a signaling protein involved in immune cell regulation that causes an increase in the production of cellular H_2O_2.[47,48]

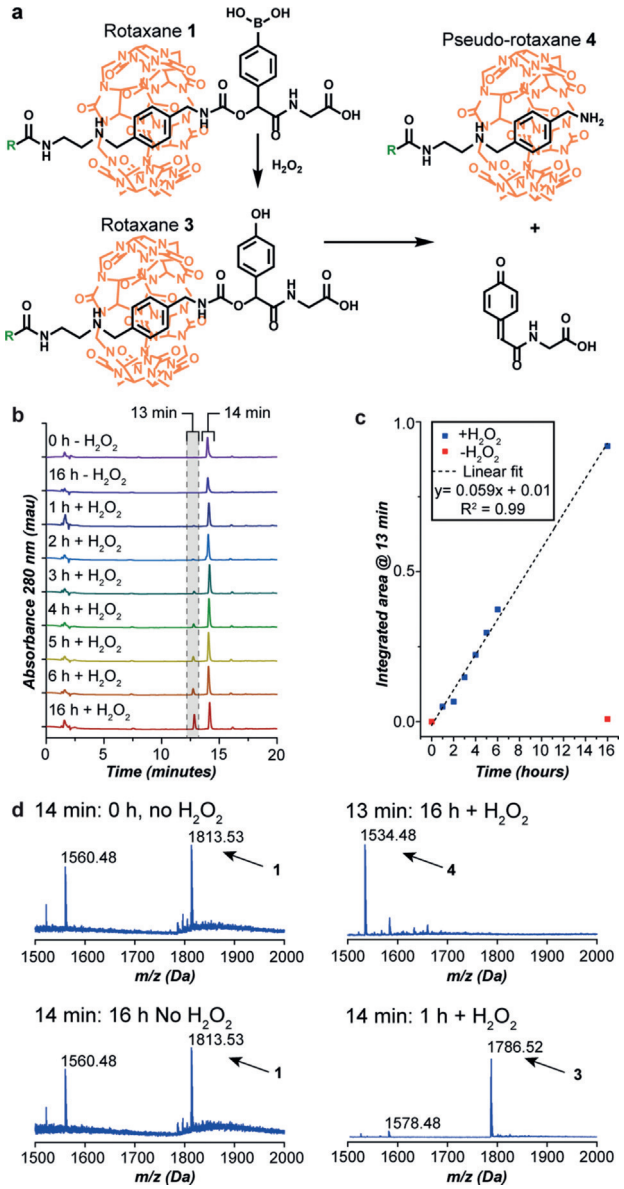

Figure 3. HPLC and ESI-TOF MS analysis of rotaxane cleavage by H_2O_2. a) The method of cleavage by H_2O_2 is shown for rotaxane **1**. b) HPLC analyses monitoring the absorbance over the course of 16 h. A control sample with no H_2O_2 added was used to determine if any degradation of the rotaxane occurred. The starting rotaxane **1** and oxidized rotaxane **3** both eluted at 14 min, but could be distinguished using ESI-TOF MS. The signal that emerges at 13 min was identified as the cleaved pseudorotaxane **4**. c) Integration of the signal area at 13 min afforded a linear relationship with respect to time. d) MS analysis of the peak at 13 min is shown: expected *m*/*z*: 1534.43; observed *m*/*z*: 1534.48. MS analysis of the peak at 14 min corresponded to the intact rotaxane, with the boronic acid group present only in samples that had not been exposed to H_2O_2 (0 and 16 h time points). In all samples that had been exposed to H_2O_2, the MS trace corresponded solely to the oxidized phenol rotaxane (expected *m*/*z*: 1785.62; observed *m*/*z*: 1786.52).

Adherent cells in six well plates were either exposed to 40 μg of TNF (TNF+) or remained untreated (TNF−). Both samples were incubated for 6 h at 37 °C under an atmosphere of 5 % CO_2. The supernatant was then treated with the TMV–

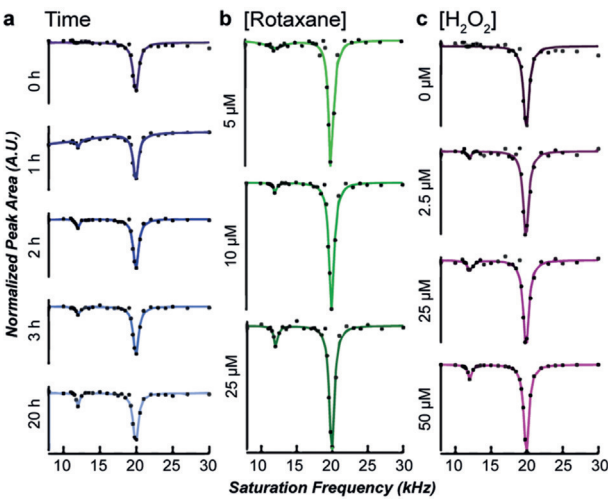

Figure 4. Rotaxane **2** acts as a ^{129}Xe hyperCEST NMR probe for H_2O_2. a) The signal at 20 kHz corresponds to bulk dissolved xenon in water and is always present, but upon addition of H_2O_2, the cleavage of rotaxane **2** releases CB6. This leads to the immediate appearance of a Xe@CB6 CEST response at 12 kHz that builds over time. b,c) The signal can be observed down to 5 μM rotaxane **2** and 2.5 μM H_2O_2.

2 conjugate to give a final concentration of 1 μM (corresponding to 10 μM rotaxane **2** groups). The samples were examined by ^{129}Xe hyperCEST NMR spectroscopy over the course of several hours (Figure 5). No Xe@CB6 signal evolved for the

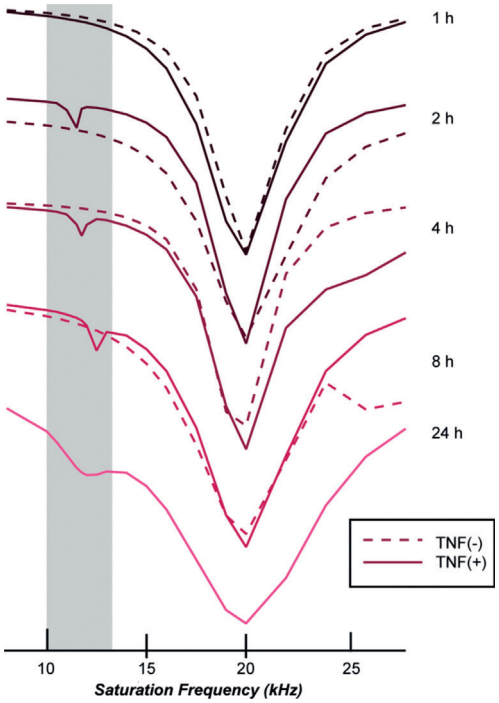

Figure 5. Detection of a ^{129}Xe hyperCEST signal in response to endogenously produced H_2O_2. TMV–**2** conjugate was added to the supernatants from HEK 293T cells with (TNF+) or lacking (TNF−) TNF in the cultures. The samples were monitored for a Xe@CB6 CEST response over 24 h. No Xe@CB6 response appeared for any of the TNF(−) samples, while a signal at 10–13 kHz appeared and stabilized within a few hours for the TNF+ samples.

TNF− sample, even after 8 h. In contrast, a response evolved and stabilized after 2 h for the TNF + sample. The Xe@CB6 signal, albeit significantly broadened, persisted even after 24 h. By comparison with the experiment in which exogenous H_2O_2 was added to HEK 293T cells, we estimate low micromolar levels of H_2O_2 were expressed as a result of incubation with TNF. This is well within the detection limit of both the sensor and target, thus demonstrating the utility of this technique to detect biologically relevant concentrations.

In conclusion, we have demonstrated the synthesis of a novel CB6 rotaxane that enables the selective detection of endogenously produced H_2O_2 by ^{129}Xe hyperCEST NMR spectroscopy. These results provide an important foundation for future applications focusing on the diagnostic imaging of diseased tissue in which peroxide levels are abnormally increased.

Acknowledgements

This work was supported by the UCSF Hana Jabsheh Fund. S.H.K. was supported by the Chemical Biology Graduate Program at UC Berkeley (NIH T32-GM066698). J.A.F. was supported under contract FA9550-11-C-0028 and awarded by the Department of Defense, Air Force Office of Scientific Research, National Defense Science and Engineering Graduate (NDSEG) Fellowship, 32 CFR 168a.

Conflict of interest

The authors declare no conflict of interest.

Keywords: cucurbit[6]uril · NMR spectroscopy · rotaxanes · sensors · xenon

How to cite: *Angew. Chem. Int. Ed.* **2019**, *58*, 9948–9953
Angew. Chem. **2019**, *131*, 10053–10058

[1] P. Caravan, *Chem. Soc. Rev.* **2006**, *35*, 512.
[2] J. Y. Park, M. J. Baek, E. S. Choi, S. Woo, J. H. Kim, T. J. Kim, J. C. Jung, K. S. Chae, Y. Chang, G. H. Lee, *ACS Nano* **2009**, *3*, 3663–3669.
[3] D. Ye, A. J. Shuhendler, P. Pandit, K. D. Brewer, S. S. Tee, L. Cui, G. Tikhomirov, B. Rutt, J. Rao, *Chem. Sci.* **2014**, *5*, 3845.
[4] A. R. Lippert, K. R. Keshari, J. Kurhanewicz, C. J. Chang, *J. Am. Chem. Soc.* **2011**, *133*, 3776–3779.
[5] G. Angelovski, S. Gottschalk, M. Milošević, J. Engelmann, G. E. Hagberg, P. Kadjane, P. Andjus, N. K. Logothetis, *ACS Chem. Neurosci.* **2014**, *5*, 360–369.
[6] C. Witte, M. Kunth, J. Döpfert, F. Rossella, L. Schröder, *J. Vis. Exp.* **2012**, *67*, e4389.
[7] Y. Wang, I. J. Dmochowski, *Acc. Chem. Res.* **2016**, *49*, 2179–2187.
[8] E. B. Adamson, K. D. Ludwig, D. G. Mummy, S. B. Fain, *Phys. Med. Biol.* **2017**, *62*(13), R81—R123.
[9] T. G. Walker, W. Happer, *Rev. Mod. Phys.* **1997**, *69*, 629–642.
[10] A. M. Oros, N. J. Shah, *Phys. Med. Biol.* **2004**, *49*, R105.
[11] K. Bartik, M. Luhmer, J.-P. Dutasta, A. Collet, J. Reisse, *J. Am. Chem. Soc.* **1998**, *120*, 784–791.
[12] M. M. Spence, S. M. Rubin, I. E. Dimitrov, E. J. Ruiz, D. E. Wemmer, A. Pines, S. Q. Yao, F. Tian, P. G. Schultz, *Proc. Natl. Acad. Sci. USA* **2001**, *98*, 10654–10657.
[13] K. K. Palaniappan, R. M. Ramirez, V. S. Bajaj, D. E. Wemmer, A. Pines, M. B. Francis, *Angew. Chem. Int. Ed.* **2013**, *52*, 4849–4853; *Angew. Chem.* **2013**, *125*, 4949–4953.
[14] C. C. Slack, J. A. Finbloom, K. Jeong, C. J. Bruns, D. E. Wemmer, A. Pines, M. B. Francis, *Chem. Commun.* **2017**, *53*, 1076–1079.
[15] Y. Wang, I. J. Dmochowski, *Chem. Commun.* **2015**, *51*, 8982–8985.
[16] S. J. Barrow, S. Kasera, M. J. Rowland, J. del Barrio, O. A. Scherman, *Chem. Rev.* **2015**, *115*, 12320–12406.
[17] B. S. Kim, Y. H. Ko, Y. Kim, H. J. Lee, N. Selvapalam, H. C. Lee, K. Kim, *Chem. Commun.* **2008**, 2756.
[18] F. T. Hane, T. Li, P. Smylie, R. M. Pellizzari, J. A. Plata, B. DeBoef, M. S. Albert, Uril, *Sci. Rep.* **2017**, *7*, 41027.
[19] C. J Bruns, J. F. Stoddart, *The Nature of the Mechanical Bond: From Molecules to Machines*, Wiley, Hoboken, **2016**, p. 761.
[20] C. J. Bruns, J. F. Stoddart, *Acc. Chem. Res.* **2014**, *47*, 2186–2199.
[21] J. A. Finbloom, C. C. Slack, C. J. Bruns, K. Jeong, D. E. Wemmer, A. Pines, M. B. Francis, *Chem. Commun.* **2016**, *52*, 3119–3122.
[22] Y. Wang, B. W. Roose, J. P. Philbin, J. L. Doman, I. J. Dmochowski, *Angew. Chem. Int. Ed.* **2016**, *55*, 1733–1736; *Angew. Chem.* **2016**, *128*, 1765–1768.
[23] A. E. Truxal, L. Cao, L. Isaacs, D. E. Wemmer, A. Pines, *Chem. Eur. J.* **2019**, *25*, 6108–6112.
[24] F. T. Hane et al., *ACS Omega* **2018**, *3*, 677–681.
[25] T. P. Szatrowski, C. F. Nathan, *Cancer Res.* **1991**, *51*, 794–798.
[26] N. Houstis, E. D. Rosen, E. S. Lander, *Nature* **2006**, *440*, 944–948.
[27] D. Nowak, M. Kasielski, A. Antczak, T. Pietras, P. Bialasiewicz, *Respir. Med.* **1999**, *93*, 389–396.
[28] E. Majewska, M. Kasielski, R. Luczynski, G. Bartosz, P. Bialasiewicz, D. Nowak, *Respir. Med.* **2004**, *98*, 669–676.
[29] F. L. Muller, W. Song, Y. C. Jang, Y. Liu, M. Sabia, A. Richardson, H. Van Remmen, *Am. J. Physiol. Regul. Integr. Comp. Physiol.* **2007**, *293*, R1159–R1168.
[30] P. Niethammer, C. Grabher, A. T. Look, T. J. Mitchison, *Nature* **2009**, *459*, 996–999.
[31] S. Reuter, S. C. Gupta, M. M. Chaturvedi, B. B. Aggarwal, *Free Radical Biol. Med.* **2010**, *49*, 1603–1616.
[32] R. Weinstain, E. N. Savariar, C. N. Felsen, R. Y. Tsien, *J. Am. Chem. Soc.* **2014**, *136*, 874–877.
[33] D. Lee, S. Khaja, J. C. Velasquez-Castano, M. Dasari, C. Sun, J. Petros, W. R. Taylor, N. Murthy, *Nat. Mater.* **2007**, *6*, 765–769.
[34] G. C. Van de Bittner, E. A. Dubikovskaya, C. R. Bertozzi, C. J. Chang, *Proc. Natl. Acad. Sci. USA* **2010**, *107*, 21316–21321.
[35] D. Srikun, E. W. Miller, D. W. Domaille, C. J. Chang, *J. Am. Chem. Soc.* **2008**, *130*, 4596–4597.
[36] V. Carroll, B. W. Michel, J. Blecha, H. VanBrocklin, K. Keshari, D. Wilson, C. J. Chang, *J. Am. Chem. Soc.* **2014**, *136*, 14742–14745.
[37] V. S. Lin, B. C. Dickinson, C. J. Chang, *Methods Enzymol.* **2013**, *526*, 19–43.
[38] P. Nikolaou, et al., *Proc. Natl. Acad. Sci.* **2013**, *110*, 14150–14155.
[39] C. Meschke, H. J. Buschmann, E. Schollmeyer, *Thermochim. Acta* **1997**, *297*, 43–48.
[40] H. J. Buschmann, L. Mutihac, R. C. Mutihac, E. Schollmeyer, *Thermochim. Acta* **2005**, *430*, 79–82.
[41] O. Danylyuk, V. P. Fedin, V. Sashuk, *Chem. Commun.* **2013**, *49*, 1859–1861.
[42] Y. Chen, M. Molnár, L. Li, P. Friberg, L.-M. Gan, H. Brismar, Y. Fu, *PLoS One* **2013**, *8*, e83805.
[43] M. Schlesinger, G. Bendas, *Int. J. Cancer* **2015**, *136*, 2504–2514.

[44] J. A. Finbloom, K. Han, I. L. Aanei, E. C. Hartman, D. T. Finley, M. T. Dedeo, M. Fishman, K. H. Downing, M. B. Francis, *Bioconjugate Chem.* **2016**, *27*, 2480 – 2485.
[45] J. Finbloom, I. Aanei, J. Bernard, S. Klass, S. Elledge, K. Han, T. Ozawa, T. Nicolaides, M. Berger, M. Francis, *Nanomaterials* **2018**, *8*, 1007.
[46] G. Adriani, M. D. de Tullio, M. Ferrari, F. Hussain, G. Pascazio, X. Liu, P. Decuzzi, *Biomaterials* **2012**, *33*, 5504 – 5513.
[47] S. J. Dixon, B. R. Stockwell, *Nat. Chem. Biol.* **2014**, *10*, 9 – 17.
[48] U. E. Martinez-Outschoorn, Z. Lin, C. Trimmer, N. Flomenberg, C. Wang, S. Pavlides, R. G. Pestell, A. Howell, F. Sotgia, M. P. Lisanti, *Cell Cycle* **2011**, *10*, 2504 – 2520.

Manuscript received: March 21, 2019
Accepted manuscript online: April 19, 2019
Version of record online: June 11, 2019

